Mutual Capacitive Flexible Tactile Sensor for 3-D Image Control

Yung-Chen Wang, Tsun-Yi Chen, Rongshun Chen, and Cheng-Yao Lo

***Abstract*—This study develops a novel mutual capacitive tactile sensor for a touch panel with shifted finger-type electrodes with high sensitivity and other benefits. This tactile sensor detects normal, shear, and pulling forces with good simultaneous visible transmittance and flexibility for the next generation of 3-D flexible portable displays. The tactile sensor is composed of polyethylene terephthalate, gold, indium tin oxide, and polydimethylsiloxane. It exhibits 75% transmittance on average in the visible region, 0.04-N force resolution, and 1.5-pF/N responsiveness. The finger-type electrode design improves sensitivity by 112%–4100%, depending on the number of fingers and shifted direction. This study conducts theoretical calculations, simulations, fabrication, and measurements. [2012-0243]**

***Index Terms*—Flexible, normal force, pulling force, shear force, tactile sensor, touch panel.**

I. Introduction

FLEXIBLE electronic devices such as paper batteries [1], [2], organic lighting [3], [4], solar cells [5], [6], thin-film transistors [7], [8], medical diagnostic equipment [9], [10], and displays [11], [12] have attracted research attention because of their low cost, high throughput, large areas, and reduced environmental impact. Of these devices, because of its multimedia applications, the flexible display is more attractive than other flexible electronic devices. Electrophoretic [13], [14], electrowetting [15], [16], electrochromic [17], [18], and microelectromechanical systems [19], [20] all have specific applications. Portable information display systems, such as cell phones and tablet computers, are rapidly replacing conventional devices such as televisions and desktop computers. Because of this trend, a flexible display device with compatible functions that is lighter, smaller, and more attractive with a larger display area than current devices is a next-generation solution. The market has begun to demand novel visual experiences, such as 3-D viewing and virtual reality. Successfully controlling a 3-D virtual image from a flat or flexible display device relies on image or gesture recognition [21], [22]. However, image or gesture recognition is inapplicable when a flexible display device is carried and held by both hands. Thus, a touch pad or keyboard should appear somewhere on a flexible display device to control a 3-D virtual image from an ergonomic perspective.

Another important factor that influences control of 3-D virtual images by using a touch pad with a flexible display device is that the touch pad must sense both horizontal (x- and y-directions) and vertical (z-direction) finger movements. Currently, touch pads for flat panel display devices use mainly resistive [23], capacitive [24], infrared-sensitive [25], inductive [26], and surface acoustic [27] techniques. Capacitive touch panels account for most of the market share because they are more sensitive than resistive and inductive panels. Capacitive touch panels can be divided into surface capacitance [28] and projected capacitance [29] mechanisms, and self-capacitance [30] and mutual capacitance [31] methods have recently been used in touch panel devices. However, when fingers move on a mutual capacitive touch panel, the sensing system and algorithm can sense only horizontal movements. The normal (vertical) force, which senses 3-D virtual image forward and backward movements, is not distinguished. This limits its applications for 3-D display and interaction possibilities between the user and a 3-D display.

Many studies have focused on fabricating flexible tactile sensors [32]–[35] with various designs and functions. However, none have successfully manufactured a flexible touch panel system with good transparency, flexibility, and sensitivity that can sense normal and shear forces (pulling or pushing) simultaneously. Therefore, this study proposes and develops a mutual capacitive flexible touch panel for next-generation displays and their applications. The touch panel is highly sensitive, has good transparency, and uses finger-type electrodes and multilayer electrodes composed of metal and indium tin oxide (ITO), respectively.

II. Structure and Operation Principles

This study focuses on a handheld display device. Thus, many design dimensions were based on human dimensions, such as fingertip size and movement distance. The demonstrative capacitance array was composed of 16 capacitors, as shown in Fig. 1(a).

Manuscript received August 28, 2012; revised December 14, 2012; accepted January 19, 2013. Date of publication March 6, 2013; date of current version May 29, 2013. This work was supported in part by the National Science Council, Taiwan, under Grant 99-2221-E-007-001-MY3 and Grant 99-2218-E-007-018-MY2 and in part by the National Tsing Hua University's "Toward a World-Class University Project." Subject Editor E. S. Kim.

Y.-C. Wang is with the Department of Power Mechanical Engineering, National Tsing Hua University, Hsinchu 30013, Taiwan, and also with the Mechanical and Systems Research Laboratories, Industrial Technology Research Institute, Hsinchu 30013, Taiwan (e-mail: robin35322@yahoo.com.tw).

T.-Y. Chen is with the Department of Power Mechanical Engineering, National Tsing Hua University, Hsinchu 30013, Taiwan (e-mail: d9633809@oz.nthu.edu.tw).

R. Chen and C.-Y. Lo are with the Department of Power Mechanical Engineering and the Institute of NanoEngineering and MicroSystems, National Tsing Hua University, Hsinchu 30013, Taiwan (e-mail: rchen@pme.nthu.edu.tw; chengyao@mx.nthu.edu.tw).

Color versions of one or more of the figures in this paper are available online at http://ieeexplore.ieee.org.

Digital Object Identifier 10.1109/JMEMS.2013.2245402

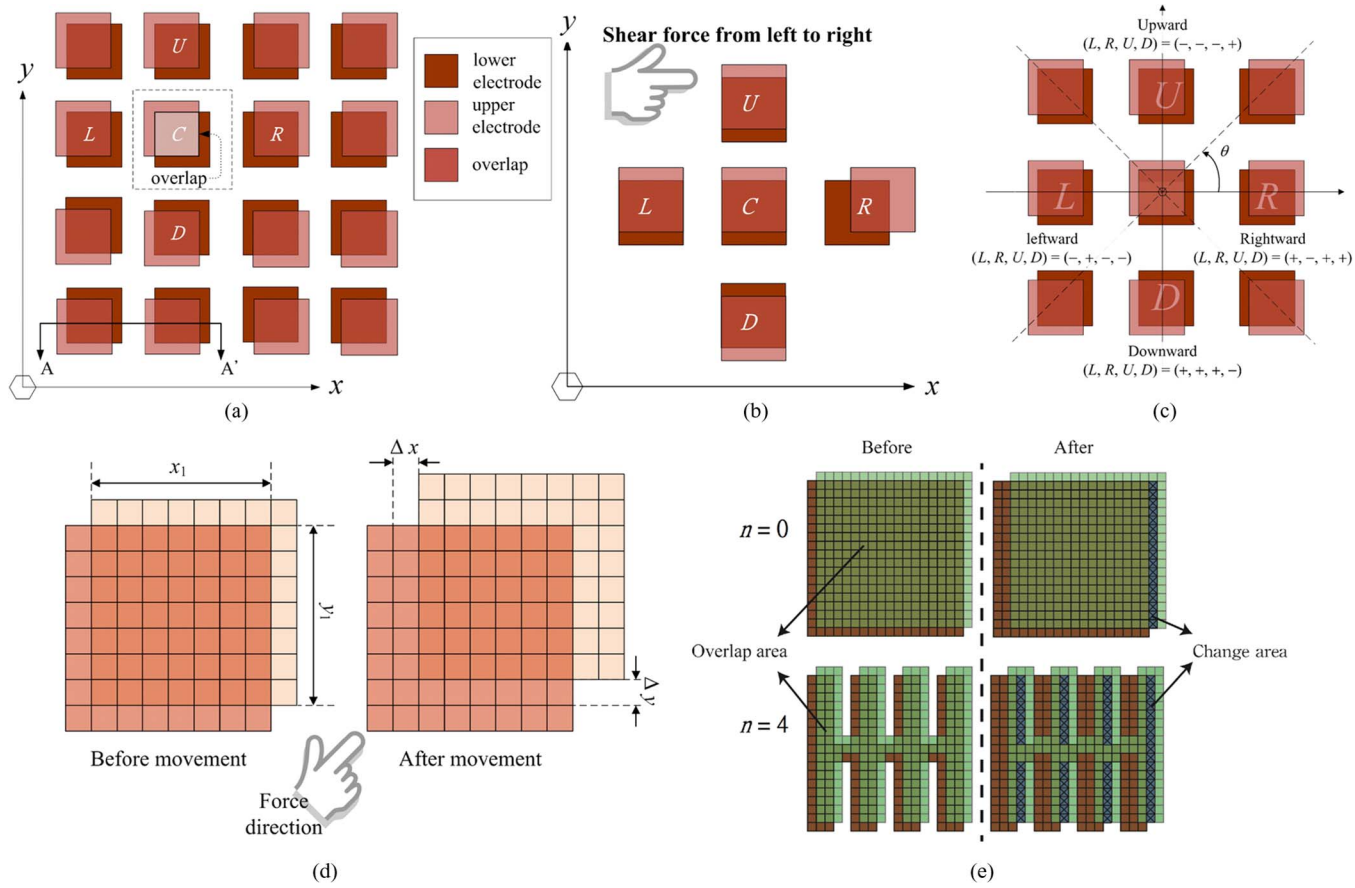

Fig. 1. Schematic plots of (a) the top view of the shifted electrode design, (b) the relative electrode movement with a left-to-right shear force, (c) the planar angle definition and simple indications for four directions, (d) the definition of the x- and y-direction movements, and (e) the finger-type electrode design using electrode R as an example. Fig. 2 shows a cross section of AA′. Each electrode in the lower and upper layers was designed with a finger-type structure, and their corresponding shift directions are shown in (a). The electrode size is 3.5 mm × 3.5 mm, and the original intentionally shifted dimension is 100 μm in both directions.

A. Shifted Mutual Capacitor

As shown in Fig. 1(a), the novel design of the mutual capacitor shifts the upper electrode array outward from its center. The aerial view clearly shows the shift in the x- and y-directions and areas of the overlap. The original overlap areas of the 16 capacitors are the same and represent the same initial capacitance values (c) with no applied force. Inside the array, any capacitor can be treated as the center (C) capacitor, and the peripheral up (U), down (D), left (L), and right (R) capacitors are referential pairs. When a normal force was applied to a capacitor, the distance between two electrodes decreased and resulted in a capacitance increase. The largest increase occurred at the target capacitor. Its peripheral capacitors experienced a smaller or even no increase, which helped the algorithm judge the size and location of the applied force. Fig. 1(b) shows a shear force applied at the center and a movement from left to right. When the upper layer was pushed slightly rightward, overlap areas C, U, D, and L increased $(+)$, and overlap area R decreased $(-)$. Because the capacitance value is positively related to its overlap area, an algorithm easily judges the movement direction and absolute shear force after comparing capacitance values with initial values. Table I lists a typical combination of referential pairs and their directions. The simulation section describes the algorithm.

TABLE I
DIRECTION IDENTIFICATION EXAMPLES OF HOW CAPACITANCE CHANGED

Moving Direction	Capacitor (+: Increase in area; −: Decrease in area.) Left (L)	Right (R)	Up(U)	Down(D)
Upward	−	−	−	+
Downward	+	+	+	−
Leftward	−	+	−	−
Rightward	+	−	+	+

Using capacitor R in Fig. 1(c) as an example, shear force angles are calculated using trigonometry

$$c_{R2} = \frac{\varepsilon(x_1 - \Delta x) \times (y_1 - \Delta y)}{d}$$
$$c_{L2} = \frac{\varepsilon(x_1 + \Delta x) \times (y_1 - \Delta y)}{d}$$
$$c_{U2} = \frac{\varepsilon(x_1 + \Delta x) \times (y_1 - \Delta y)}{d}$$
$$c_{D2} = \frac{\varepsilon(x_1 + \Delta x) \times (y_1 + \Delta y)}{d} \quad (1)$$

where C_{R2}, C_{L2}, C_{U2}, and C_{D2} represent the capacitance values after movement for pairs R, L, U, and D, respectively.

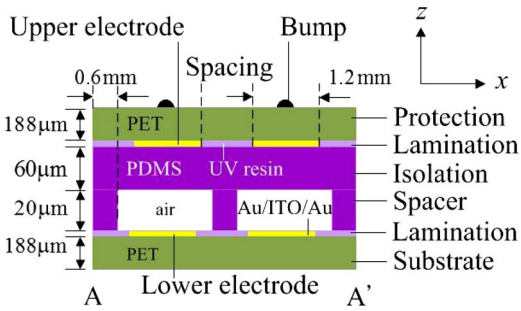

Fig. 2. Cross-sectional schematic plot of two capacitors with materials and their dimensions from AA′ in Fig. 1(a).

In (1), ε, x_1, y_1, Δx, Δy, and d represent the dielectric air constant, overlap length in direction x, overlap length in direction y, overlap length difference in direction x, overlap length difference in direction y, and isolation thickness, respectively. Fig. 1(d) shows their corresponding meanings. Because the upper and lower layers were bonded by fixed elastomer spacers ($x_1 \gg \Delta x$ and $y_1 \gg \Delta y$), the movement was assessed using

$$\left|\frac{c_{D2}-c_{U2}}{c_{L2}-c_{R2}}\right| = \left|\frac{\Delta y(x_1+\Delta x)}{\Delta x(y_1-\Delta y)}\right| \approx \frac{x_1 \Delta y}{y_1 \Delta x}. \quad (2)$$

Because the intentionally shifted capacitance array had equal initial overlap lengths in x- and y-directions ($x_1 = y_1$), the shear force angle (θ) was

$$\theta = \tan^{-1}\left(\left|\frac{c_{D2}-c_{U2}}{c_{L2}-c_{R2}}\right|\right) = \tan^{-1}\left(\frac{\Delta y}{\Delta x}\right). \quad (3)$$

B. Advanced Finger-Type Electrode

After a conventional mutual capacitance design with an intentionally shifted overlap area, a finger-type electrode design was introduced for each capacitance electrode to enhance sensitivity. As shown in Fig. 1(e), electrode areas were divided into smaller areas, but they were still connected to each other. This allowed the total overlay length to be simply hypothesized by multiplying it by its number of fingers (n). In Fig. 1(e), $n = 4$. Because the capacitance value is positively related to its area and the algorithm only calculates capacitance change (Δc), the sensitivity of this advanced design could also be enhanced.

III. Simulation

Fig. 2 shows a schematic drawing of the cross-sectional structure in Fig. 1(a). The touch panel was composed of a lower layer (including the substrate, lower electrode, and lamination), a spacer layer (including the spacer and air gap), and an upper layer (including the isolation, upper electrode, lamination, and protection). Commercial software COMSOL (version 4.0) used the electromechanical coupling function for simulations on a 3×3 capacitance array, as shown in Fig. 1(c).

During the simulation, boundary conditions were set for the lower layer to ensure that all lower layer elements were fixed in all directions. The temperature was set to 300 K, and force was applied to the center capacitor (C). This section verifies the concept of the intentionally shifted electrode design and evaluates the finger-type design.

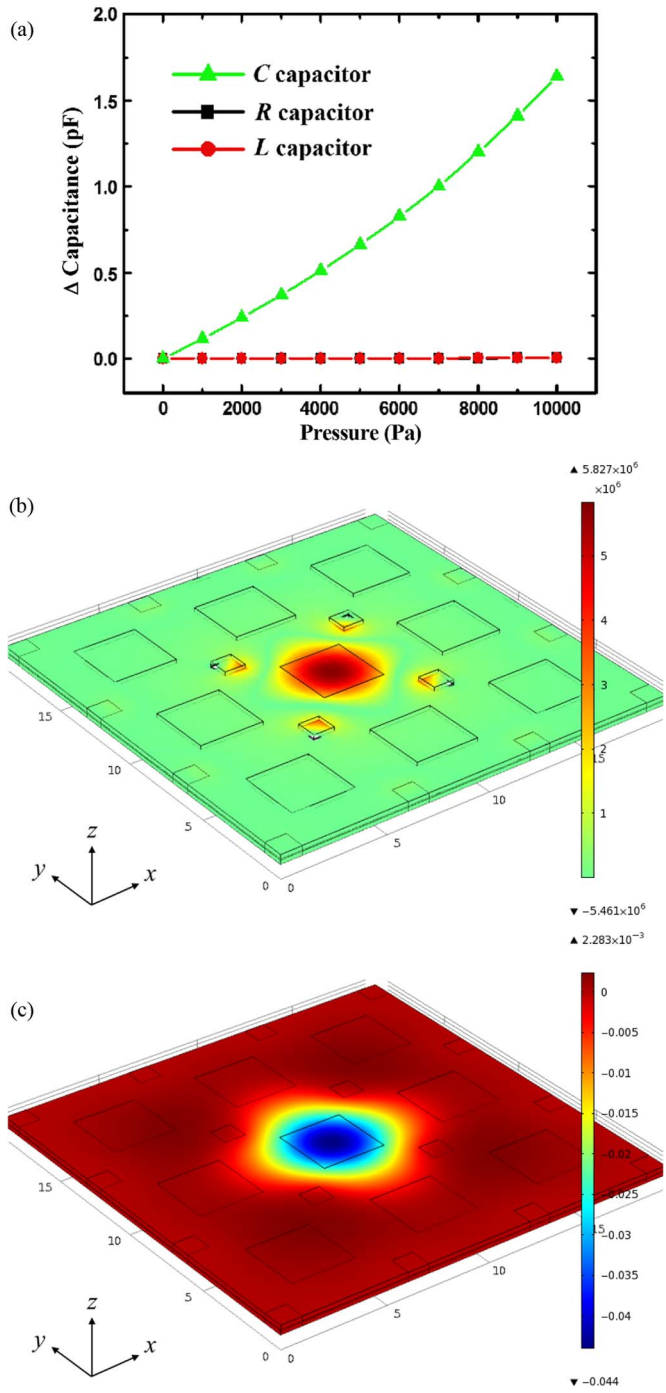

Fig. 3. (a) Simulated capacitance change in the left (L), center (C), and right (R) capacitors under normal force, (b) distribution of a normal force applied to the center capacitor of a 3×3 array (units are in pascals), and (c) displacement in the z-direction on the 3×3 array (units are in micrometers).

A. Shifted Mutual Capacitor Simulation: Normal Force

Fig. 3(a) shows the simulation results of capacitance change (Δc) along the applied normal force (F) of 10 000 Pa. The capacitance of the center capacitor gradually increased, whereas that of the right and left capacitors did not. Because the algorithm only judged Δc, the results in Fig. 3(a) imply that the center capacitor provided sufficient change, whereas either the other two capacitors did not deform or their deformations were negligible. Fig. 3(b) shows a simulated displacement in the

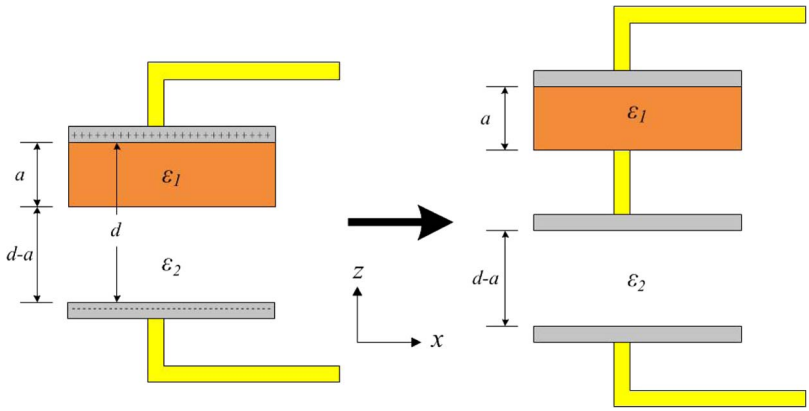

Fig. 4. Capacitors in series for a single electrode pair.

z-direction. Because the force was applied to the center capacitor, stress accumulated mainly at the center, but the surrounding locations also experienced minor stress. This simulation result informed the design of electrode and spacing dimensions between capacitors. Small spacing provides more sensitivity for fingertip movement but also generates noise when determining which capacitor is touched. Large spacing reduces target capacitor location errors but reduces the sensing resolution of high-definition displays. Fig. 2 shows the optimized design.

The linearity of the center capacitor was unexpected: Capacitance change Δc increased exponentially instead of increasing linearly as implied by the capacitance equation $c = \varepsilon A/d$, where A is the overlap area and the other parameters are the same as those in (1). This is because the capacitor in this study uses a complex insulating material consisting of an isolation and an air gap. The material between the two electrodes in Fig. 2 can be decomposed into two capacitors in series, as shown in Fig. 4, and the complex capacitance becomes

$$c = \frac{\varepsilon_0 A}{\frac{d}{\varepsilon_1} + \frac{d-a}{\varepsilon_2}} \tag{4}$$

where ε_0, ε_1, ε_2, and a represent the dielectric constant in a vacuum, relative dielectric constant of the isolation, relative dielectric constant of air, and isolation thickness, respectively. The serial connection results show that total capacitance increased nonlinearly although applied force increased linearly.

B. Shifted Mutual Capacitor Simulation: Shear Force

Fig. 5(a) shows the simulation results of a shear force that was applied from D to U. Unlike peripheral capacitor behavior under a normal force, D and U show an inverse trend, which implies an increasing overlap area in U and a decreasing overlap area in D. Because the shear force consists of a lateral and a normal force and the normal force also increased along with the shear force, the capacitance of C increased slightly instead of decreasing during operation. The inset in Fig. 5(a) explains the shear force decomposition, and Fig. 5(b) shows simulated displacement in the y-direction.

C. Advanced Finger-Type Electrode Simulation

Finger-type electrodes can enhance capacitance change, producing a highly sensitive touch panel. Fig. 6 shows the simulation results for R in Fig. 1(a) with a finger-type design and an 80 000-Pa shear force from left to right. The touch panel with this advanced design showed a larger capacitance change, and this capacitance change was positively related to the applied force. However, capacitance change increased nonlinearly with the number of fingers. As shown in Fig. 1(d) and (e), when the number of fingers increases, the total increases in x_1 and y_1 are unequal. Using the $\theta = 45^\circ$ shear force in Fig. 1(e) as an example, the delta overlap area changes (ΔA) of $n = 3$ and $n = 4$ are 62 and 69 units, respectively. A unit represents a square area in the figure. Although the number of fingers increased from three to four, ΔA only increased by only $69/62 = 1.11$, which is less than the number-of-finger ratio $(4/3 = 1.33)$. Table II shows this nonlinear unit increase and implies that different enhancement behaviors appear if the shifted electrode occurs in different corners of Fig. 1(e). The numbers in brackets are the unit increment ratios of $n = 3$ or $n = 4$ to $n = 2$. This corrects the previous hypothesis and implies that, when pattern numbers increase, the enhancement effect weakens. Nevertheless, because the relationship between applied force and capacitance change was positive, using $n \geq 2$ to replace the original design was expected to enhance its effect. This study uses $n = 4$ in the following sections.

In the minimal enhancement case, the overlap area difference ratio was $19/17 = 112\%$, which occurred on the bottom-right $\theta = 315^\circ$ shift. In the maximal enhancement case, the overlap area difference ratio was $41/1 = 4100\%$, which occurred on the top-left $\theta = 135^\circ$ shift.

IV. Materials and Processes

A. Material Selection and Specifications

As shown in Fig. 2, the touch panel was composed of several different materials. Polyethylene terephthalate (PET; Toray T60) with a thickness of 188 μm was selected as the substrate and protection. PET is well known for its low price and good visible-region transmittance. Therefore, it is suitable for touch panel applications on display devices.

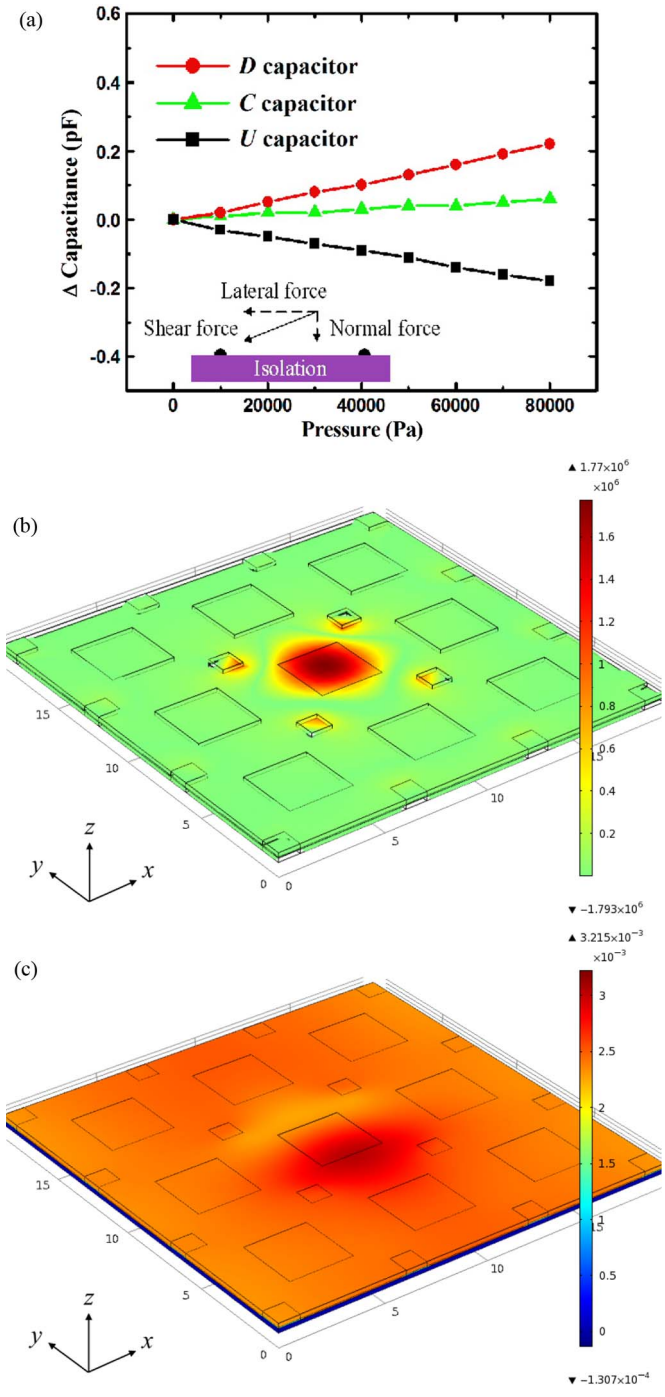

Fig. 5. (a) Simulated capacitances of left (U), center (C), and right (D) capacitors under shear force. The inset explains the shear force decomposition. (b) Distribution of the shear force applied to the center capacitor of a 3×3 array (units are in pascals). (c) Displacement in the z-direction on the same 3×3 array (units are in micrometers).

Electrodes were composed of ITO and gold (Au) because of good visible-region transmittance and good conductivity, respectively. Metal-only or ITO-only solutions cannot achieve transmittance, conductivity, and flexibility; thus, a layered stack of Au (5 nm), ITO (200 nm), and Au (5 nm) was used in the flexible touch panel. This Au–ITO–Au metal provides a $3.64 \times 10^{-5}\ \Omega \cdot \text{cm}$ resistivity.

Ultraviolet (UV)-sensitive resin (Loctite 3311) was selected for its adhesion and lamination capabilities. The UV resin also

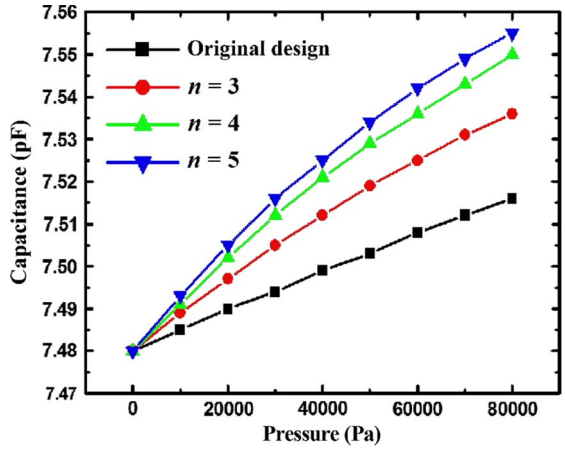

Fig. 6. Simulated capacitance with different numbers of fingers under shear forces.

provided the flatness over the Au–ITO–Au electrode after spin coating and UV exposure. During UV exposure, the UV resin solidifies and provides a bonding force between the upper and lower layers. The spin-coating process ensured that the UV resin on the Au–ITO–Au electrode and the PET substrate was 5 μm in thickness.

Polydimethylsiloxane (PDMS; Sylgard 184) was used for the isolation and spacer structures. PDMS is renowned for its low Young modulus, making it suitable for flexible electronic devices. PDMS requires a low thermal budget to solidify and is suitable for the polymer substrate in electronic devices. This study used PDMS formation on a silicon (Si) mold to define the PDMS shape. The spin-coating process ensured that the PDMS isolation layer was 60 μm, and the Si mold trench depth ensured that the PDMS spacer layer was 20 μm.

B. Process

Fig. 7 shows a schematic plot of the process. A PET substrate was sputtered (Cressington 108) with Au–ITO–Au before electrode pattern definition by photolithography. This process was used for the upper and lower layers.

During electrode patterning, a Si substrate with patterns was defined using photolithography before performing inductively coupled plasma reactive ion etching (ICPRIE; Samco RIE-10NR). After ICPRIE, the structured Si was treated with antiadhesion material (Alfa Aesar L16606) and then spin coated with PDMS. The PDMS on Si was solidified in atmospheric air at 100 °C for 30 min. The PDMS, together with the Si mold, was put on one of the previously mentioned layer with spin-coated UV resin. Because the electrode was 210 nm thick and the UV resin was 5 μm thick, the UV resin covered the electrode step height during solidification under 100-mW UV exposure (XLite 500) for 3 min. When the UV resin solidified, the PET with the electrode and isolation layer was unmolded from the Si.

Another layer done with the same process as that before was then put beneath the PDMS and was put under a second UV exposure with the sample exposure dosage. The intentionally shifted design was achieved under an optical microscope. After lamination, an inkjet printer produced bumps that enhance shear

TABLE II
NONLINEAR UNIT (SQUARE AREA) SUMMARY WITH DIFFERENT NUMBERS OF FINGERS

	Moving direction					
Number of fingers (n)	None	Right	Upper-Right	Upper-Left	Lower-Right	Lower-Left
2	83	51	35	96	64	132
3	116(1.4×)	67(1.3×)	54(1.5×)	144(1.5×)	80(1.3×)	180(1.4×)
4	157(1.8×)	86(1.7×)	82(2.3×)	192(2.0×)	92(1.4×)	228(1.7×)

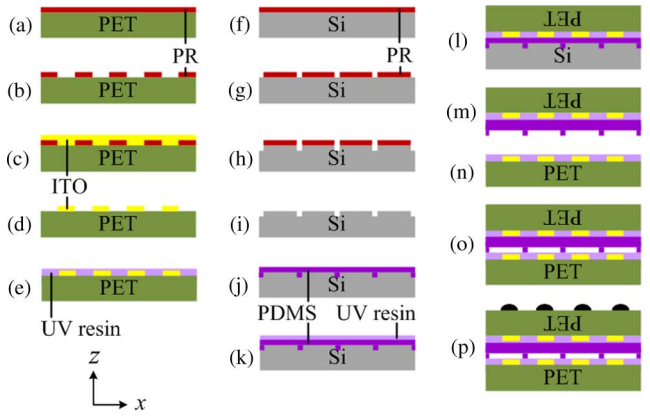

Fig. 7. Process illustration. (a) Spin coat the photoresist (PR) onto the PET substrate. (b) Pattern the PR using lithography. (c) Sputter ITO on the patterned PR. (d) Lift-off the PR, and leave the patterned ITO on the PET substrate. (e) Spin coat the UV resin on the patterned ITO. (f) Spin coat the PR on the Si substrate. (g) Pattern the PR using lithography. (h) Dry etch the Si substrates. (i) Strip off the PR. (j) Spin coat the patterned Si with PDMS, and solidify the PDMS on a hot plate. (k) Spin coat the UV resin on PDMS. (l) Flip the structure in (e) and align it with the structure in (k), and then, laminate them using UV exposure. (m) Unmold the laminated structure from the Si mold. (n) Prepare another structure from (e). (o) Align (m) and (n), and then, laminate them using UV exposure. (p) Inkjet print bumps onto each capacitor.

force. The bumps were 10-μm-high hemispheres. Previous studies have used this inkjet process [36] for similar structures. Overlap length in the x- and y-directions was thus carefully controlled.

V. DEVICE PERFORMANCE AND DISCUSSION

To verify touch panel performance, homemade force gauge, circuit, and display were used to monitor its real-time response. A capacitor multiplexer (Analog Devices ADG1208) and a controller (Microchip PIC12FJ128GB106) were used to verify the control and calculation circuit. The algorithm and signal process study was programmed using commercial software Matlab (version 2009a). Generally, sensitivity decreased as the scanning rate increased and vice versa. Final demonstrations were conducted at a 30-Hz sampling rate. Fig. 8 illustrates the measurement setup and the sensing circuits. Although the force gauge provided force with units of newtons, it transferred to the sensor through the bumps. Considering the force received by the capacitors, pressure with units of pascals should be used during measurement. In real cases of touch panel sensors, fingertips with specific area sizes also provide loadings of pressure. The relationship between force and pressure introduces a contact area with Pa $=$ N/m^2. We unify the loading of pressure for all simulations and measurements by introducing the bump size.

A. Normal Force

As shown in Fig. 9, the normal force response behaved similarly to the simulated one. The difference between the measured data resulted from the nonlinear behavior mentioned in Section III; that is, the extra capacitor in series with the structure provided the system with extra capacitance, resulting in a larger value. Tiny air bubbles trapped between the UV resin and PDMS isolation were randomly observed on electrodes. These air bubbles contributed extra capacitance to the measurement data. Therefore, the intentional air gap, together with the unintentional air bubbles, in the system contributed to this extra capacitance. This process control issue could be avoided if the lamination process in Fig. 7 was performed in a vacuum or using an automatic pressure roller. Because the mutual capacitance technique mechanism only senses capacitance change, the difference between the measured data and simulation results was negligible. The responsiveness to normal force was 1.9 pF/N, and the resolution (the minimal sensible force) was 630 Pa.

B. Shear Force

For shear force measurement, the target capacitor should be monitored, and its peripheral capacitor capacitance changes should be recorded and calculated. The shear force value was obtained from the target capacitor, but the shear force direction was obtained only from the peripheral capacitors. To understand peripheral capacitor changes, the 4 $\times$ 4 touch panel in Fig. 1(a) was enlarged to an 8 $\times$ 4 panel.

Using a right-to-left shear force as an example, the algorithm output clearly showed users where the target point was by judging its R and L references, as shown in Fig. 10 with smoothed continuous data points. Fig. 11 shows the responsiveness comparison between measured data and simulation results. Unlike the normal force, the shear force deviated from the simulation along the applied force. The simulation setting limitations explain this. During the simulation, the shear force was composed of a normal and a lateral force, which were set separately, as shown in the inset in Fig. 5(a). To vary the shear force, the normal force was constant, and the lateral force was variable. However, during real measurement, the normal and lateral forces changed, resulting in a decreasing isolation (d) and an increasing capacitance. When the applied force increased, the difference between the measured data and simulation results also increased. Therefore, the responsiveness to the normal force was 1.5 pF/N, and the resolution was 1120 Pa.

Fig. 12 shows the lateral force within a shear force and its influence on the structure. By comparing the capacitance

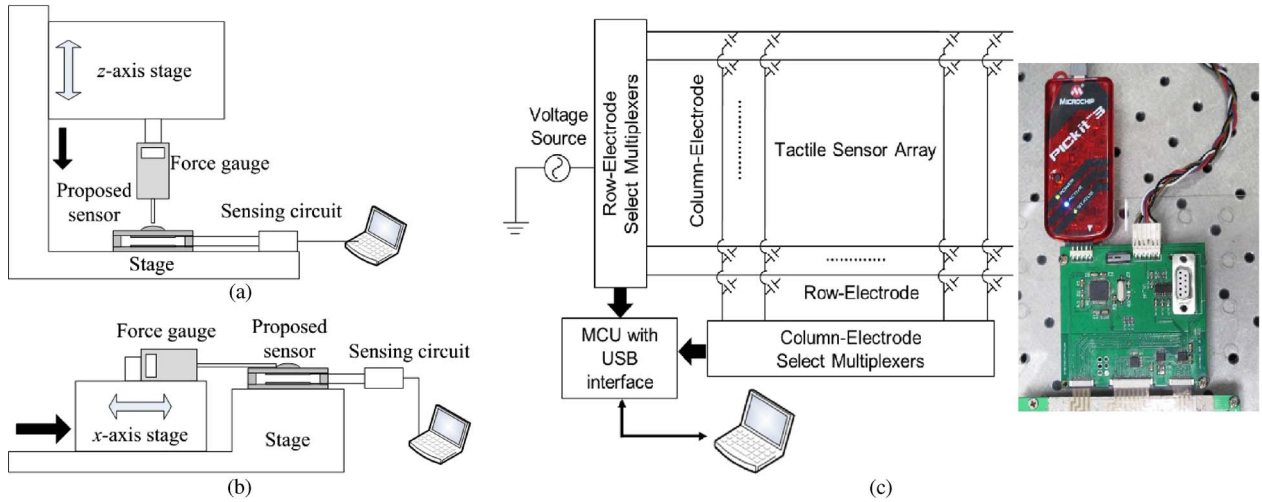

Fig. 8. Measurement setup for (a) normal and pulling force and (b) shear force detections. (c) Sensing circuit with a picture of the circuit board.

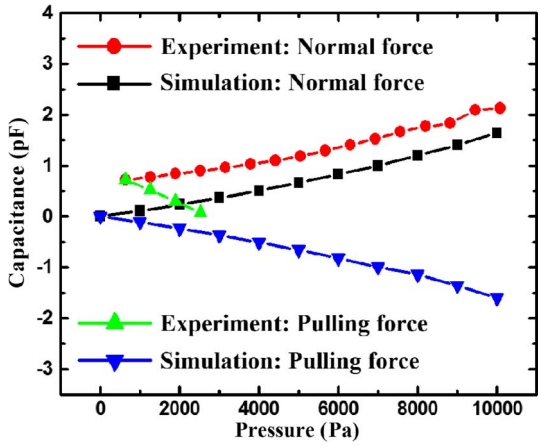

Fig. 9. Capacitance change comparison between experimental and simulated data with normal and pulling forces.

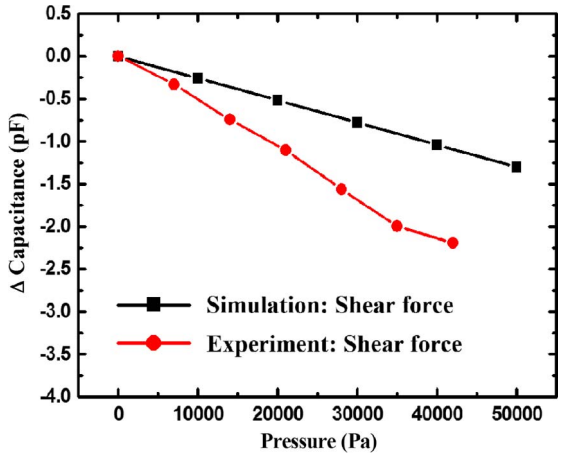

Fig. 11. Capacitance change comparison between experimental and simulated data under shear force.

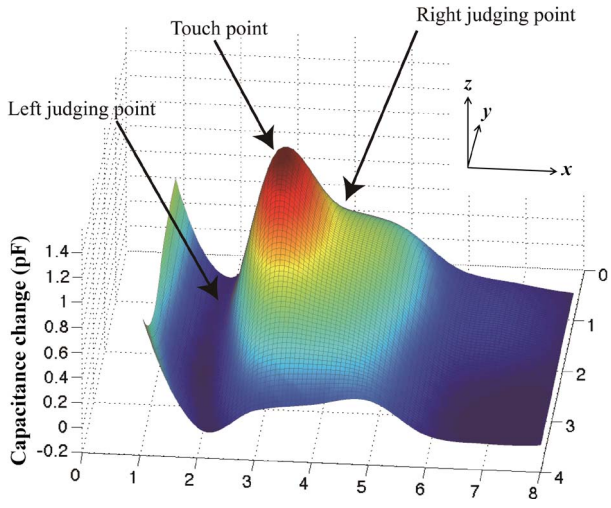

Fig. 10. Measured shear force direction and amplitude. Data points were connected and smoothed.

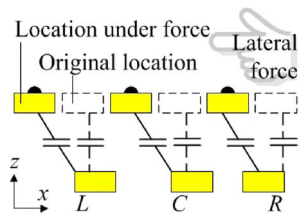

Fig. 12. Explanation of relative movement in the x-direction of the referential capacitors under shear force. The dashed boxes represent the original locations of the upper electrodes.

change in the L and R capacitors, shear force direction and value were obtained after referencing the original electrode shift directions using the algorithm.

C. Pulling Force

To test the pulling performance, the target capacitor was attached to the force gauge with commercial glue with the same size bump. This ensured that the bump was bonded strongly to the force gauge and that the force was 100% transferred to the capacitor. With this setting, no delamination or deformation related to the bump occurred. Fig. 9 shows the pulling force simulation and measurement data. The capacitance change under a pulling force behaved similarly to that under the normal force but in the opposite direction. It gradually decreased because of the space increase between two electrodes. Similar

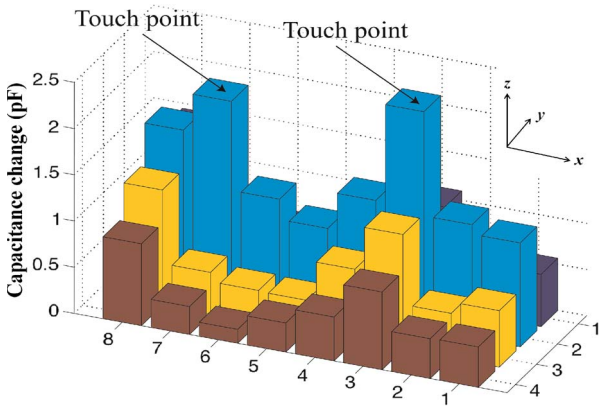

Fig. 13. Measured multitouch amplitudes and their locations.

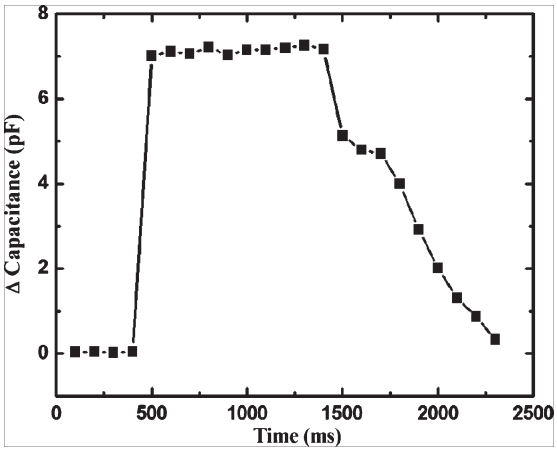

Fig. 14. Touch panel response time.

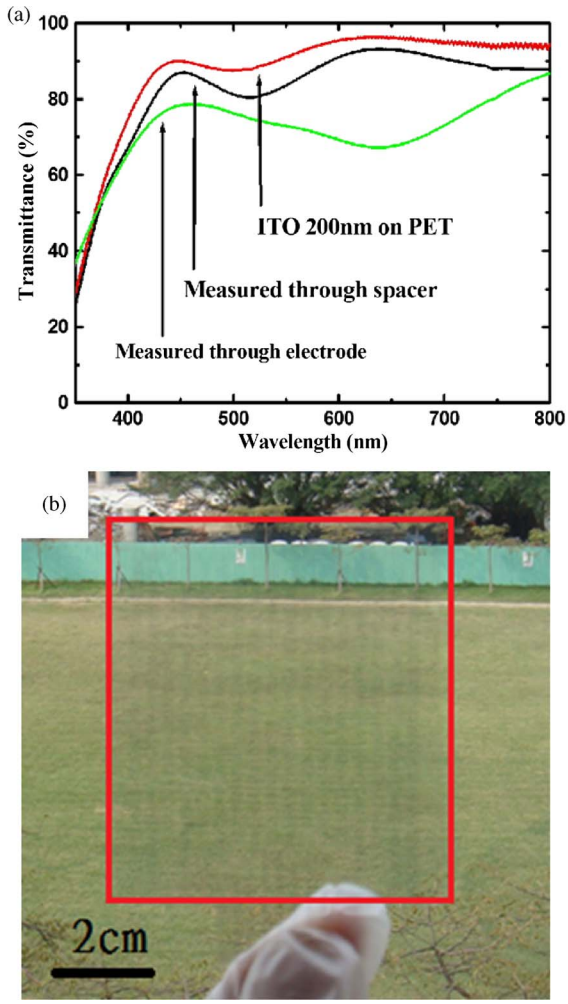

Fig. 15. (a) Transmittance measured through different regions of the touch panel structure. The ITO on PET transmittance is for comparison, and (b) the sensor array (in the red box) was visually clear with acceptable and slightly visible patterns.

to normal force, the pulling force began with a data difference that was attributed to process defects, but its value decreased more along the applied force with a larger absolute slope. The pulling force responsiveness was 5.7 pF/N, which is larger than that of the normal force case (1.9 pF/N). This could be explained by defects induced during measurement. Because the bump was strongly bonded to the gauge, the slight delamination between layers contributed extra capacitance in series. Therefore, the total capacitance and extra delamination capacitance in series decreased. Furthermore, a small pulling force range was measured before a physical breakdown of layer delamination. However, this force range and sensitivity are sufficient for touch panel applications on display devices. Lamination improvement could overcome this issue.

D. Multitouch and Response Time

Because of their intuitive control and variations, multitouch panels are essential for smart phones and tablet computers. Although the market has not demanded multiple 3-D image control, this function can be supported if the scanning circuit responds promptly. Fig. 13 shows that multiple sensing capability is possible with two target points. Fig. 14 shows the response time for a single capacitor. Response time depends on the operation circuit. The rise time was shorter than 10 ms with a 10-pF/N responsiveness. The fall time was longer than the rise time because the capacitor suffered from two limitations: structural air gap return and material isolation return. This implies that the fall time could be improved by using less flexible or larger Young modulus material for isolation. However, this could cause a tradeoff between touch panel fall time and flexibility.

E. Transmittance

This design uses a multiple-layer electrode to replace the conventional pure metal conductor. Fig. 15 shows that the multilayer design provides reasonable transmittance from the Au conductivity and ITO transmittance. The measurement was conducted at the electrode region with the lowest transmittance because of the thin metal. It was larger than 70% on average in the visible region, which is suitable for display devices, irrespective of whether it covers the display panel or appears at other locations such as touch pads or keyboards.

By combining the discussed detection methodologies, users can control an image for either 2-D or 3-D movement. For example, when three fingers (the thumb, index finger, and middle finger) simultaneously, but individually, controlled three

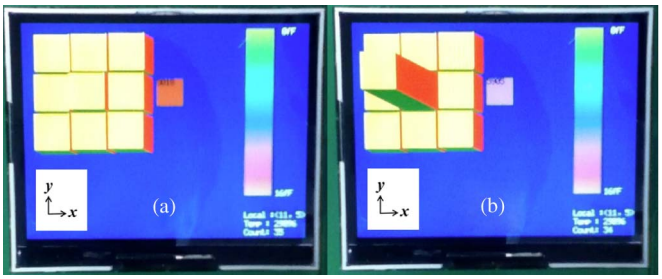

Fig. 16. Demonstrative monitors (a) without and (b) with 3-D movement.

capacitors to move an image forward, the shear force directions of the thumb, index finger, and middle finger were 270°, 135°, and 45°, respectively. The circuit sensed the normal forces, and the algorithm calculated the target electrode location. The lateral forces were decomposed from the shear and net forces with the net direction in the xy plane calculated using trigonometry. The vertical (z-direction) image movement was calculated using the same method. The 3-D movement of an image was achieved, as shown in Fig. 16. To clearly see the z-direction movement, the image and representative target (the top surface of the pillar) were tilted.

F. Sensitivity With Bending

One of the most interesting and attractive functions for displays and touch panels is their flexibility. Many studies have claimed that their functional materials were fabricated on flexible substrates with simple picture demonstration of their flexibility with unspecified radius (r) or cyclic reliability for specific materials and not the whole sensor structure [33], [37]–[42]. Other reports have mentioned material resistance change or the characteristic changes in tactile sensors when bent [34], [43] but excluded analysis on how the sensor behaves when bent. No research discusses the sensitivity of tactile sensors influenced by mechanical force. The relationships between applied force, bending radius, structure formation change, and sensitivity are uncertain. Fig. 17(a) shows the simulation results of a tactile sensing capacitor structure during bending. The top layer bumps were ignored for simplicity, which did not affect bending behaviors. The air gap decreased in the z-direction when the structure was bent, which confirms previous research results [36]. The simulation results imply a sensitivity change during bending because of the air gap change, which varied the distance between the two electrodes. The tactile sensors were carefully attached to solid molds with different bending radii and were then measured using the same methodology described in the device performance section. The sensitivity of the tactile sensor in a flat state (infinite r) is included in the figure for comparison.

Similar to those in previous studies [34], capacitance changes were larger at smaller bending radii, which implies that the reduced air gap between the two electrodes contributes to higher sensitivity. However, in contrast with the simulation results showing that the air gap decreased with bending, which increases capacitor sensitivity, the measurement results show reduced sensitivity with decreased bending radii in Fig. 17(b). This is because extra support from the bending structure successfully distributed the applied force (load) from the top in the z-direction to the bottom in the x- and y-directions. This behavior complies with the cylindrical shell model [44], where a smaller bending radius shows less displacement in the z-direction with the same load. The cylindrical shell model explains that, when the displacement is the same, a smaller bending radius structure supports heavier loads. The experiment results in Fig. 17(b) correlate with the cylindrical shell model.

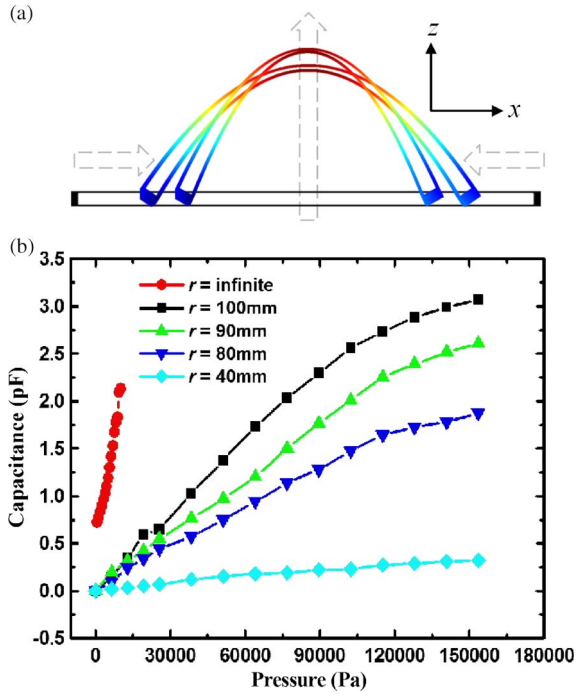

Fig. 17. (a) Simulation explaining the air gap change at different bending curvatures. The air gap at the center gradually decreased, which is implying a more sensitive capacitance change. Dashed arrows at both ends indicate the dimension retreat, and dashed arrow at the center indicates the bending trend. The air gap at the edge gradually increased because of the extension of the elastic spacer. (b) Measured capacitance with different applied forces and bending radii.

VI. Summary

This paper has proposed a mutual capacitive touch panel with a novel design (shifted electrode pairs), enhanced sensitivity (finger-type electrodes), good transmittance (Au–ITO–Au multiple layer), and good flexibility (PDMS and spacer structure), which is suitable for normal, shear, and pulling force sensing applications. A demonstration device with 1120-Pa (0.04-N) resolution and 1.5-pF/N responsiveness has been designed, simulated, and verified. Unlike devices with conventional separate-sensing mechanisms for normal and shear forces, this device senses both forces using the same structure. The device can also perform pulling force sensing functions, which expand touch panel applications. Furthermore, the device allows highly accurate novel multitouch operation. During bending, the tactile sensor sensitivity was corrected by the cylindrical shell model before evaluation. With its good transmittance, this touch panel is suitable for the next generation of display devices, such as

portable flexible displays and 3-D displays, and it allows users to move 3-D images.

REFERENCES

[1] H. Liu and R. M. Crooks, "Paper-based electrochemical sensing platform with integral battery and electrochromic read-out," *Anal. Chem.*, vol. 84, no. 5, pp. 2528–2532, Mar. 2012.

[2] L. Nyholm, G. Nyström, A. Mihranyan, and M. Strømme, "Toward flexible polymer and paper-based energy storage devices," *Adv. Mater.*, vol. 23, no. 33, pp. 3751–3769, Sep. 2011.

[3] Q.-C. Hsu, J.-J. Hsiao, T.-L. Ho, and C.-D. Wu, "Fabrication of photonic crystal structures on flexible organic light-emitting diodes using nanoimprint," *Microelectron. Eng.*, vol. 91, pp. 178–184, Mar. 2012.

[4] G. Gu, P. E. Burrows, S. Venkatesh, S. R. Forrest, and M. E. Thompson, "Vacuum-deposited, nonpolymeric flexible organic light-emitting devices," *Opt. Lett.*, vol. 22, no. 3, pp. 172–174, Feb. 1997.

[5] C.-N. Chen, C.-T. Huang, C.-L. Chao, M. T.-K. Hou, W.-C. Hsu, and J. A. Yeh, "Strengthening for sc-Si solar cells by surface modification with nanowires," *J. Microelectromech. Syst.*, vol. 20, no. 3, pp. 549–551, Jun. 2011.

[6] K. M. Coakley and M. D. McGehee, "Conjugated polymer photovoltaic cells," *Chem. Mater.*, vol. 16, no. 23, pp. 4533–4542, Nov. 2004.

[7] L. Dong, R. Yue, and L. Liu, "Fabrication and characterization of integrated uncooled infrared sensor arrays using a-Si thin-film transistors as active elements," *J. Microelectromech. Syst.*, vol. 14, no. 5, pp. 1167–1177, Oct. 2005.

[8] X. Duan, C. Niu, V. Sahi, J. Chen, J. W. Parce, S. Empedocles, and J. L. Goldman, "High-performance thin-film transistors using semiconductor nanowires and nanoribbons," *Nature*, vol. 425, no. 6955, pp. 274–278, Sep. 2003.

[9] A. W. Martinez, S. T. Phillips, B. J. Wiley, M. Gupta, and G. M. Whitesides, "FLASH: A rapid method for prototyping paper-based microfluidic devices," *Lab Chip*, vol. 8, no. 12, pp. 2146–2150, Dec. 2008.

[10] Z. Nie, C. A. Nijhuis, J. Gong, X. Chen, A. Kumachev, A. W. Martinez, M. Narovlyansky, and G. M. Whitesides, "Electrochemical sensing in paper-based microfluidic devices," *Lab Chip*, vol. 10, no. 4, pp. 477–483, Feb. 2010.

[11] S. R. Forrest, "The path to ubiquitous and low-cost organic electronic appliances on plastic," *Nature*, vol. 428, no. 6986, pp. 911–918, Apr. 2004.

[12] C. D. Sheraw, L. Zhou, J. R. Huang, D. J. Gundlach, and T. N. Jackson, "Organic thin-film transistor-driven polymer-dispersed liquid crystal displays on flexible polymeric substrates," *Appl. Phys. Lett.*, vol. 80, no. 6, pp. 1088–1090, Feb. 2002.

[13] B. Comiskey, J. D. Albert, H. Yoshizawa, and J. Jacobson, "An electrophoretic ink for all-printed reflective electronic displays," *Nature*, vol. 394, no. 6690, pp. 253–255, Jul. 1998.

[14] S. M. Venugopal and D. R. Allee, "Integrated a-Si:H source drivers for 4″ QVGA electrophoretic display on flexible stainless steel substrate," *J. Display Technol.*, vol. 3, no. 1, pp. 57–63, Mar. 2007.

[15] B. Sun, K. Zhou, Y. Lao, J. Heikenfeld, and W. Cheng, "Scalable fabrication of electrowetting displays with self-assembled oil dosing," *Appl. Phys. Lett.*, vol. 91, no. 1, pp. 011106-1–011106-3, Jul. 2007.

[16] J. Heikenfeld, K. Zhou, E. Kreit, B. Raj, S. Yang, B. Sun, A. Milarcik, L. Clapp, and R. Schwartz, "Electrofluidic displays using Young–Laplace transposition of brilliant pigment dispersions," *Nat. Photon.*, vol. 3, no. 5, pp. 292–296, May 2009.

[17] P. Andersson, R. Forchheimer, P. Tehrani, and M. Berggren, "Printable all-organic electrochromic active-matrix displays," *Adv. Funct. Mater.*, vol. 17, no. 16, pp. 3074–3082, Nov. 2007.

[18] W. A. Gazotti, G. Casalbore-Miceli, A. Geri, A. Berlin, and M. A. De Paoli, "An all-plastic and flexible electrochromic device based on elastomeric blends," *Adv. Mater.*, vol. 10, no. 18, pp. 1522–1525, Dec. 1998.

[19] C.-Y. Lo, O.-H. Huttunen, J. Hiitola-Keinänen, J. Petäjä, H. Fujita, and H. Toshiyoshi, "MEMS-controlled paper-like transmissive flexible display," *J. Microelectromech. Syst.*, vol. 19, no. 2, pp. 410–418, Apr. 2010.

[20] D. Felnhofer, K. Khazeni, M. Mignard, Y. J. Tung, J. R. Webster, C. Chui, and E. P. Gusev, "Device physics of capacitive MEMS," *Microelectron. Eng.*, vol. 84, no. 9/10, pp. 2158–2164, Sep. 2007.

[21] A. Erol, G. Bebis, M. Nicolescu, R. D. Boyle, and X. Twombly, "Vision-based hand pose estimation: A review," *Comput. Vis. Image Understand.*, vol. 108, no. 1/2, pp. 52–73, Oct. 2007.

[22] Y. Zhu and G. Xu, "A real-time approach to the spotting, representation, and recognition of hand gestures for human–computer interaction," *Comput. Vis. Image Understand.*, vol. 85, no. 3, pp. 189–208, Mar. 2002.

[23] M. H. Ahn, E.-S. Cho, and S. J. Kwon, "Effect of the duty ratio on the indium tin oxide (ITO) film deposited by in-line pulsed DC magnetron sputtering method for resistive touch panel," *Appl. Surf. Sci.*, vol. 258, no. 3, pp. 1242–1248, Nov. 2011.

[24] I.-S. Yang and O.-K. Kwon, "A touch controller using differential sensing method for on-cell capacitive touch screen panel systems," *IEEE Trans. Consumer Electron.*, vol. 57, no. 3, pp. 1027–1032, Aug. 2011.

[25] S. Y. Han, K. S. Jeon, B. Cho, M. S. Seo, J. Song, and H.-S. Kong, "Characteristics of a-SiGe:H thin film transistor infrared photosensor for touch sensing displays," *IEEE J. Quantum Electron.*, vol. 48, no. 7, pp. 952–959, Jul. 2012.

[26] K. Kurita, Y. Fujii, and K. Shimada, "A new technique for touch sensing based on measurement of current generated by electrostatic induction," *Sens. Actuators A, Phys.*, vol. 170, no. 1/2, pp. 66–71, Nov. 2011.

[27] J. T. Du, W. L. Li, H. A. Xu, and Z. G. Liu, "Vibro-acoustic analysis of a rectangular cavity bounded by a flexible panel with elastically restrained edges," *J. Acoust. Soc. Amer.*, vol. 131, no. 4, pp. 2799–2810, Apr. 2012.

[28] T. G. Zimmerman, J. R. Smith, J. A. Paradiso, D. Allport, and N. Gershenfeld, "Applying electric field sensing to human–computer interfaces," in *Proc. SIGCHI Conf. Human Factors Comput. Syst.*, New York, NY, USA, 1995, pp. 280–287.

[29] T.-H. Hwang, W.-H. Cui, I.-S. Yang, and O.-K. Kwon, "A highly area-efficient controller for capacitive touch screen panel systems," *IEEE Trans. Consum. Electron.*, vol. 56, no. 2, pp. 1115–1122, May 2010.

[30] H.-K. Lee, S.-I. Chang, and E. Yoon, "Dual-mode capacitive proximity sensor for robot application: Implementation of tactile and proximity sensing capability on a single polymer platform using shared electrodes," *IEEE Sensors J.*, vol. 9, no. 12, pp. 1748–1755, Dec. 2009.

[31] K. Kim, K. Shin, J.-H. Han, K.-R. Lee, W.-H. Kim, K.-B. Park, B.-K. Ju, and J. J. Pak, "Deformable single wall carbon nanotube electrode for transparent tactile touch screen," *Electron. Lett.*, vol. 47, no. 2, pp. 118–120, Jan. 2011.

[32] A. D. Mazzeo, W. B. Kalb, L. Chan, M. G. Killian, J.-F. Bloch, B. A. Mazzeo, and G. M. Whitesides, "Paper-based, capacitive touch pads," *Adv. Mater.*, vol. 24, no. 21, pp. 2850–2856, Jun. 2012.

[33] R. D. P. Wonga, J. D. Posnerb, and V. J. Santos, "Flexible microfluidic normal force sensor skin for tactile feedback," *Sens. Actuators A, Phys.*, vol. 179, pp. 62–69, Jun. 2012.

[34] S. Takamatsu, T. Takahata, M. Muraki, E. Iwase, K. Matsumoto, and I. Shimoyama, "Transparent conductive-polymer strain sensors for touch input sheets of flexible displays," *J. Micromech. Microeng.*, vol. 20, no. 7, p. 075017, Jul. 2010.

[35] J. Engel, J. Chen, and C. Liu, "Development of polyimide flexible tactile sensor skin," *J. Micromech. Microeng.*, vol. 13, no. 3, pp. 359–366, May 2003.

[36] Y.-R. Huang, S.-A. Kuo, M. Stach, C.-H. Liu, K.-H. Liao, and C.-Y. Lo, "A high sensitivity three-dimensional-shape sensing patch prepared by lithography and inkjet printing," *Sensors*, vol. 12, no. 4, pp. 4172–4186, Mar. 2012.

[37] H.-K. Lee, S.-I. Chang, and E. Yoon, "A flexible polymer tactile sensor: Fabrication and modular expandability for large area deployment," *J. Microelectromech. Syst.*, vol. 15, no. 6, pp. 1681–1686, Dec. 2006.

[38] P. Peng and R. Rajamani, "Flexible microtactile sensor for normal and shear elasticity measurements," *IEEE Trans. Ind. Electron.*, vol. 59, no. 12, pp. 4907–4913, Dec. 2012.

[39] Y.-F. Lan, W.-C. Peng, Y.-H. Lo, and J.-L. He, "Durability under mechanical bending of the indium tin oxide films deposited on polymer substrate by thermionically enhanced sputtering," *Org. Electron.*, vol. 11, no. 4, pp. 670–676, Apr. 2010.

[40] Y. S. Kim, W. J. Hwang, K. T. Eun, and S.-H. Choa, "Mechanical reliability of transparent conducting IZTO film electrodes for flexible panel displays," *Appl. Surf. Sci.*, vol. 257, no. 18, pp. 8134–8138, Jul. 2011.

[41] S.-H. Choa, C.-K. Cho, W.-J. Hwang, K. T. Eun, and H.-K. Kim, "Mechanical integrity of flexible InZnO/Ag/InZnO multilayer electrodes grown by continuous roll-to-roll sputtering," *Sol. Energy Mater. Sol. Cells*, vol. 95, no. 12, pp. 3442–3449, Dec. 2011.

[42] J. W. Seo, J.-W. Park, K. S. Lim, S. J. Kang, Y. H. Hong, J. H. Yang, L. Fang, G. Y. Sung, and H.-K. Kim, "Transparent flexible resistive random access memory fabricated at room temperature," *Appl. Phys. Lett.*, vol. 95, no. 13, pp. 133508-1–133508-3, Oct. 2009.

[43] W.-Y. Chang, T.-H. Fang, S.-H. Yeh, and Y.-C. Lin, "Flexible electronics sensors for tactile multi-touching," *Sensors*, vol. 9, no. 2, pp. 1188–1203, Feb. 2009.

[44] J. N. Reddy, "Theory and analysis of shells," in *Theory and Analysis of Elastic Plates and Shells*. Boca Raton, FL, USA: CRC Press, 2007, pp. 430–441.

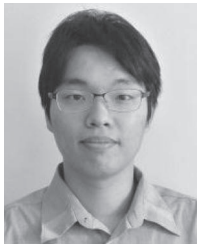

Yung-Chen Wang received the B.S. degree in mechanical engineering from National Chung Cheng University, Chiayi, Taiwan, in 2007 and the M.S. degree in mechanical engineering from National Chiao Tung University, Hsinchu, Taiwan, in 2009.

He is currently an Engineer with the Mechanical and Systems Research Laboratories, Industrial Technology Research Institute, Hsinchu. His current research interests include flexible electronic and embedded systems.

Tsun-Yi Chen received the B.S. degree in mechanical engineering from National Chung Cheng University, Minxiong, Taiwan, in 2005 and M.S. degree in mechanical engineering from the National Chiao Tung University, Hsinchu, Taiwan, in 2007. He is currently working toward the Ph.D. degree in the Department of Power Mechanical Engineering, National Tsing Hua University, Hsinchu.

His current research interests are flexible electronic devices, microelectromechanical systems, and control systems.

Rongshun Chen received the Ph.D. degree in mechanical engineering from the University of Michigan, Ann Arbor, MI, USA, in 1992.

He is currently a Professor with the Department of Power Mechanical Engineering and the Institute of NanoEngineering and MicroSystems, National Tsing Hua University, Hsinchu, Taiwan. His research interests include microelectromechanical systems, integration and control of microsystems, and nanoimprinting.

Dr. Chen is a member of the IEEE Control Systems Society, IEEE Circuits and Systems Society, and IEEE Electron Devices Society.

Cheng-Yao Lo received the Ph.D. degree in electrical engineering from The University of Tokyo, Tokyo, Japan, in 2009.

During 2001–2005, he was a Senior R&D Process Integration Engineer with Taiwan Semiconductor Manufacturing Company, where he was responsible for the process development of 90- and 45-nm technologies. During 2006–2009, he was a Visiting Researcher with the VTT Technical Research Centre of Finland, where he was responsible for the large-area-printed microelectromechanical systems display project. Since 2010, he has been an Assistant Professor with the Institute of NanoEngineering and MicroSystems, National Tsing Hua University, Hsinchu, Taiwan, where he has also been an Adjunct Professor with the Department of Power Mechanical Engineering since 2012. His current research interest is flexible printed electronic devices and processes.